Physics of the Solid State, 2023, Vol. 65, No. 10

06,13

Fabrication of the $BiFeO_3/Sr_{0.6}Ba_{0.4}Nb_2O_6/SrRuO_3/MgO(001)$ heterostructure, as well as features of its crystal structure, surface morphology, and physical properties

© D.V. Stryukov[1], Ya.Yu. Matyash[1], N.V. Strilec[1], A.V. Pavlenko[1], N.V. Malomyzheva[2]

[1] Southern Scientific Center, Russian Academy of Sciences,
Rostov-on-Don, Russia
[2] Scientific Research Institute of Physics, Southern Federal University,
Rostov-on-Don, Russia
E-mail: strdl@mail.ru

Received August 1, 2023
Revised August 1, 2023
Accepted August 3, 2023

Studies of the crystal structure, surface nanostructure, and properties of the $BiFeO_3/Sr_{0.6}Ba_{0.4}Nb_2O_6/SrRuO_3/MgO(001)$ heterostructure were carried out. Nanosized $SrRuO_3$(25 nm), $Sr_{0.6}Ba_{0.4}Nb_2O_6$(100 nm), and $BiFeO_3$(100 nm) films were deposited sequentially on a MgO(001) substrate by RF-cathode sputtering in an oxygen atmosphere. It has been established that there are no impurity phases in the fabricated heterostructure, all layers are grown heteroepitaxially, and the deformation of the unit cell in the upper $BiFeO_3$ layer was 0.28%. It has been shown that during the deposition of each subsequent layer in the series of MgO(001) → SRO → SBN60 → BFO, the surface roughness of the upper film increases from 0.292 nm to 2.977 nm, but the maximum lateral crystallite size is observed for SBN60. The revealed regularities and features in the analysis of the magnetic and ferroelectric properties of the heterostructure obtained by magnetic force microscopy and atomic force microscopy are discussed.

Keywords: bismuth ferrite, $BiFeO_3$, SBN60, X-ray diffraction, atomic force microscopy.

DOI: 10.61011/PSS.2023.10.57224.171

1. Introduction

Currently, the ever-growing demand for faster and multifunctional microelectronic devices resulted in great interest in the study of thin-film structures based on promising functional materials, such as multiferroics (materials with two or more „ferro“ orders) [1,2]. Besides, for environmental reasons, the choice of material is subject to restrictions on the use of lead-free compounds. Among single-phase lead-free multiferroics, the most famous and promising material is bismuth ferrite ($BiFeO_3$, or BFO). BFO has high temperatures of ferroelectric ($T_C \approx 1100\,K$) and antiferromagnetic ($T_N \approx 640\,K$) phase transitions [3]. At room temperature and without deformation BFO has a rhombohedral (R) unit cell with R3c space group, in which the polar axis is directed along the [111] pseudocubic direction. BFO manufacturing in the form of thin films allows both to obtain a significant magnetic response due to the destruction of a spatially modulated magnetic structure, and to create the unit cell strain. At sufficiently large biaxial deformations the rhombohedral structure of the ground state can transform into a tetragonal-like (T)-phase under compressive strain [4,5], or into an orthorhombic (O)-phase under tensile strain [6]. One of the important features of BFO is that it can withstand large strain, for example, in BFO films on $LaAlO_3$ it is possible to achieve an unprecedented unit cell strain up to 4.67 Å compared to the bulk parameter of 3.96 Å [4,5] and a great tetragonal distortion coefficient $c/a = 1.23$. Such great strain and radical change in symmetry lead to both change in the BFO properties and to a number of new phenomena, such as large ferroelectric polarization [7], elastic-optical effect [8] and abnormal photovoltaic effect [9]. Bulk BFO has unprecedented values of polarization $\approx 100\,\mu C/cm^2$ in direction of polar axes, and in case of T phase the polarization reaches $\approx 130\,\mu C/cm^2$ [7]. Besides, the rhombohedral and tetragonal phases can transform into each other by applying the electric field, allowing BFO multiferroic thin film to exhibit a strong piezoelectric effect, which can be used, for example, in actuators and acoustic sensors. Thus, BFO has great potential for application in various multifunctional devices.

The creation of two-layer heterostructures is, on the one hand, a way to control strain in the layers, and on the other hand, the interaction between layers can lead to new effects [11,12]. In combination with BFO films, in this paper we consider barium strontium niobate ($Sr_xBa_{1-x}Nb_2O_6$ or SBNx), which has the tetragonal tungsten bronze structure with P4bm space group [13] and, unlike to BFO, is characterized, for example, by high pyroelectric activity and large values of dielectric constant and controllability in the vicinity of room temperatures [14]. Thin SBN films were already successfully epitaxially deposited onto various substrates, including MgO(001). Considering the high sensitivity of BFO to unit cell strain, as well as the large piezoelectric coefficient and uniaxiality of SBN, when they are combined into a two-layer heterostructure, one should expect both changes in properties compared to single-layer structures and strong influence of the external electric field. The purpose of this paper was to establish the patterns of phase composition, crystal structure, nanostructure, ferroelectric and magnetic properties of $BiFeO_3/Sr_{0.6}Ba_{0.4}Nb_2O_6/SrRuO_3/MgO(001)$ using X-ray diffraction and atomic force microscopy methods.

2. Objects. Manufacturing and research methods

Nanosized films of the BFO/SBN60/SRO/MgO(001) heterostructure were grown by RF cathode sputtering in oxygen atmosphere on „Plazma 50 SE" units. The ceramic disks of stoichiometric compositions $BiFeO_3$, $Sr_{0.6}Ba_{0.4}Nb_2O_6$ and $SrRuO_3$ with a 50 mm diameter and 3 mm thick were used as targets. Prepared for heteroepitaxial deposition 0.5 mm thick (001) cut MgO plates (OST Photonics, China, double-sided polishing) were used as substrate. Sputtering was carried out in three stages, where at the first stage a 25 nm thick $SrRuO_3$ layer was deposited onto the MgO substrate. Then the substrate was cooled to room temperature, and only after cooling the second layer of SBN60 100 nm thick was deposited. Before depopsition of the last 100 nm thick BFO layer, the substrate was also cooled to room temperature. The substrate temperature at the beginning of sputtering of each layer was — 400°C, the pressure of pure oxygen in the chamber was — 67 Pa, the distance between the target and the substrate was — 12 mm.

X-ray diffraction studies were carried out on multifunctional X-ray complex „RICOR" (Bragg–Brentano geometry, goniometer with increment up to 0.001° (Crystal Logic Inc.); X-ray tube BSV 21-Cu (JSC „Svetlana-Rentgen"), scintillation detector (LLC ITC „Radikon").

The surface morphology of the heterostructure was studied in semi-contact and contact modes on an atomic-force microscope (AFM) „Ntegra Academia" (NT-MDT Spectrum Instruments, Russia) using a silicon cantilever NS15/50 (NT-MDT Spectrum Instruments, Russia, hardness — 40 N/m, probe rounding radius — 8 nm). Scanning of the surface relief fragment of $5 \times 5\,\mu m^2$ size with a resolution of 300 points per line was carried out at a 1 Hz rate in semi-contact mode. Using a silicon cantilever NSG01 with Pt coating (NT-MDT Spectrum Instruments, Russia, hardness — 5 N/m, probe rounding radius — 30 nm) in the Kelvin probe force microscopy (KPFM) the surface potential of the film from pre-polarized areas was recorded. The magnetic properties of the heterostructures were studied using two-pass magnetic force microscopy (MFM). The magnetic cantilever MFM01 (NT-MDT Spectrum Instruments, Russia, hardness — 3 N/m, probe rounding radius — 8 nm) was used. The second pass was performed with the cantilever retracted by 50–70 nm depending on the surface roughness. The oscillation amplitude was 0.3 V. Processing and analysis of the received scans were carried out in the Image Analysis software.

3. Experimental results and discussion

According to X-ray diffraction analysis, it was established that there are no impurity phases in the BFO/SBN60/SRO/MgO(001) and SBN60/SRO/MgO(001) heterostructures. Considering that the $\theta-2\theta$ X-ray diffraction patterns (Figure 1) of both samples contain only reflections from planes of (00l) family for each layer of the heterostructure and MgO substrate, we can conclude that [001] axis is co-directed in BFO, SBN60, SRO layers, which are parallel to the [001] axis of MgO substrate.

Each maximum (00l) in $\theta-2\theta$ X-ray diffraction patterns of the SBN60/SRO/MgO(001) heterostructure was double, corresponding to separate scattering of SBN60 and SRO layers. Sputtering BFO layer on top caused the maxima (00l) to become triple, where additional third line corresponded to the BFO layer scattering. From the maxima positions of each component of the reflection decomposition, the unit cells parameters of each layer of BFO/SBN60/SRO/MgO(001) heterostructure were determined, where $c_{\text{SRO}} = 0.3973$ nm, $c_{\text{SBN60}} = 0.3961$ nm, $c_{\text{BFO}} = 0.3976$ nm. The parameters are determined with an accuracy of 10^{-4} nm. Comparison of received parameters for BFO layer with parameters for bulk BFO ceramics ($c_{\text{bulk}} = 3.965$ Å, $\alpha = 89.4°$) shows that in the heterostructure the unit cell of BFO layer is stretched, and BFO unit cell strain ($\varepsilon = (c_{\text{film}} - c_{\text{bulk}})/c_{\text{bulk}} \times 100\%$) is 0.28%. The magnitude of the vertical misorientation of the [001] crystallographic axes for BFO and SBN60 layers was determined using rocking curves for the most intense (002) reflections (insert in Figure 1). The vertical misorientation for BFO and SBN60 layers does not exceed 1.3°. φ-scans of (221) reflections of SBN60 layer, (101) of BFO layer and (113) of MgO substrate (Figure 2) were obtained. The X-ray patterns of the heterostructure layers show clear maxima, which proves the epitaxial growth of BFO and SBN60 layers.

In φ-X-ray pattern of the (221) reflections of SBN60 layer, 8 maxima are visible, similar to the SBN61/MgO(001) films, the angular positions of which indicate the formation of orientation domains rotated symmetrically by +18.4° and −18.4° relative to the axes of the MgO substrate. In this case, the angular positions of (101) reflections on φ-X-ray patterns for BFO layer (Figure 2) relative to the positions of the maxima of (113) MgO substrate reflections indicate the parallel the crystallographic axes of BFO layer and MgO substrate. The observed shift of reflections by 45° is due to the choice of (113) and (103) reflections for φ-scanning. The azimuthal misorientation, determined by the width at half maximum of the reflections on φ-X-ray patterns, did not exceed 2.3° for BFO layer, and 2.6° — for SBN60 layer.

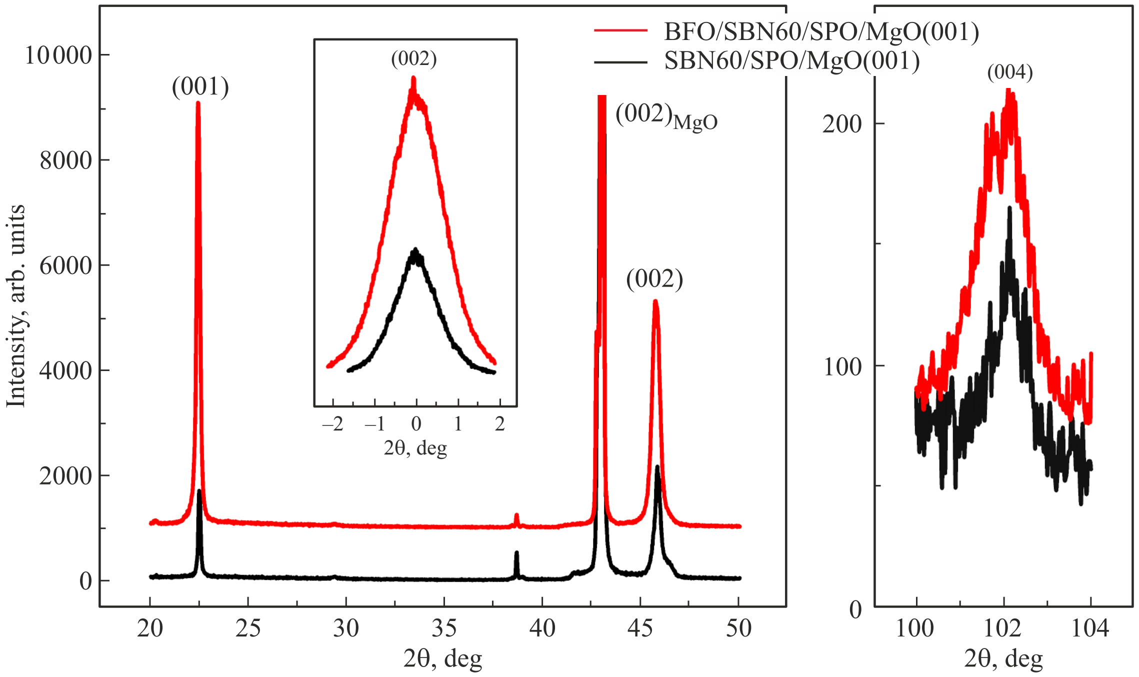

Figure 1. $\theta{-}2\theta$ X-ray patterns of BFO/SBN60/SRO/MgO(001) and SBN60/SRO/MgO(001) heterostructures. The insert shows the rocking curves of (002) reflection of the heterostructures.

Thus, low values of vertical and azimuthal misorientation, small width of X-ray reflections and high intensity for nanosized layers indicate the high quality and structural perfection of the obtained objects. Another interesting fact is that the crystallographic axes of BFO are parallel to the axes of MgO substrate, despite the fact that BFO layer is grown on SBN60 surface, while in the SBN60 structure the formation of orientation domains with a rotation of the crystallographic axes ±18.4° was detected.

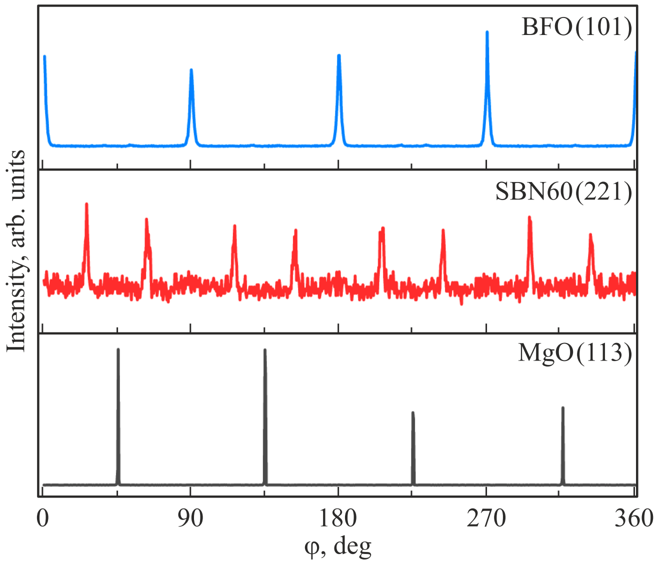

Figure 2. X-ray φ-scan of (101) reflections of BFO layer, (221) SBN60 layer, and (113) MgO substrate for BFO/SBN60/SRO/MgO(001) heterostructures.

Parameters of surface materials according to AFM data

Sample	Sq, nm	Sa, nm	St, nm	Sp, nm	Sv, nm
MgO	0.292	0.233	2.470	1.191	1.279
SRO/MgO	0.353	0.281	2.623	1.288	1.335
SBN/SRO/MgO	2.460	2.043	13.759	5.315	8.444
BFO/SBN/SRO/MgO	2.977	2.390	19.708	9.614	10.093

Note. Sq — root mean square surface roughness; Sa — average roughness; St — distance between maximum height and maximum depth; Sp —max height; Sv — maximum depth.

The results of studying the surface morphology of single-crystal MgO substrate, SRO/MgO, SBN60/SRO/MgO and BFO/SBN60/SRO/MgO heterostructures are presented in Figure 3 and in the Table.

From three-dimensional images of the samples surface it is clear that as each subsequent layer is deposited, the surface relief of the heterostructure increases, but a certain trend is distinguished. Thus, if the surface of MgO substrate prepared for heteroepitaxial deposition was atomically smooth with value of root mean square roughness (Sq)$\sim$ 0.295 nm, then after 25 nm thick SRO film deposition the roughness increased, but root mean square roughness value remained low ($\sim$ 0.353 nm). The surface relief of SBN60 film was more complex in comparison with SRO, the difference in heights and depressions increased from 2.6 to 13.7 nm, and it was formed by growth blocks

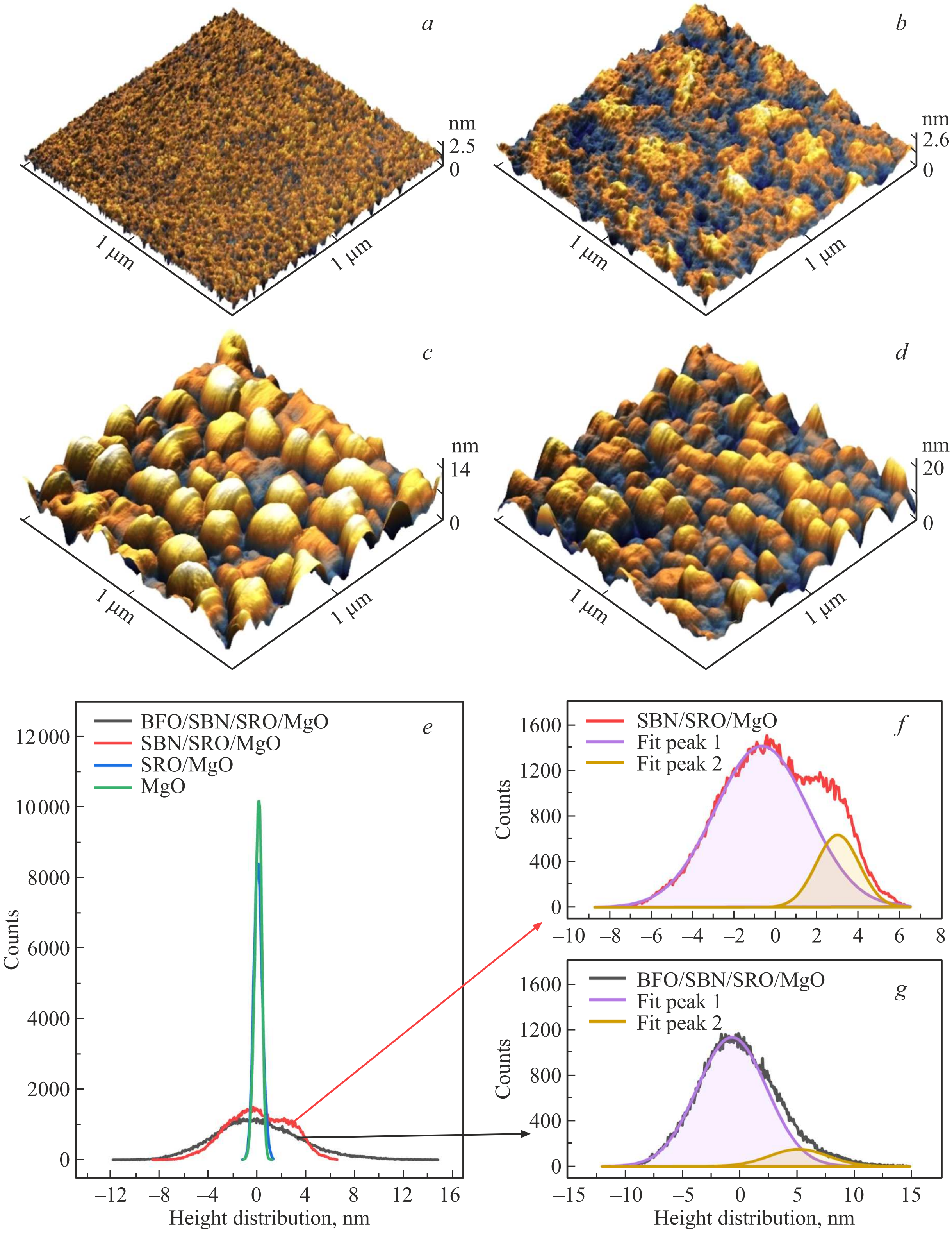

Figure 3. 3D surface image of MgO (*a*), SRO/MgO (*b*), SBN60/SRO/MgO (*c*), and BFO/SBN60/SRO/MgO (*d*) heterostructures. *e*–*g* — histograms of height distribution in the analyzed areas with fragment $4\,\mu m^2$.

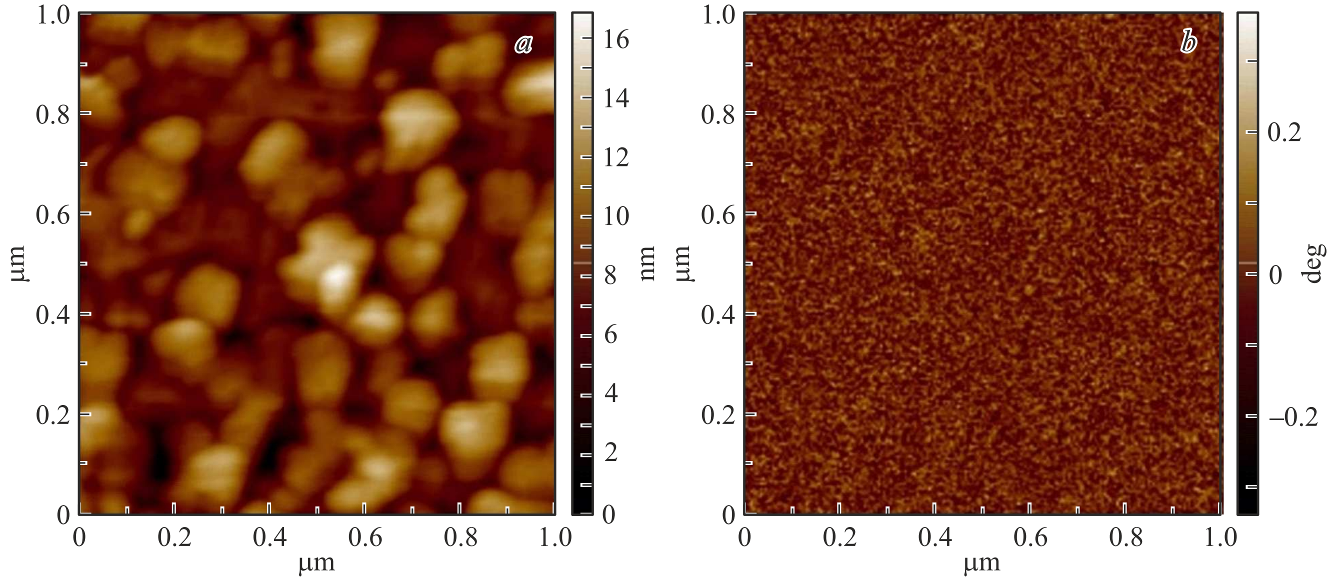

Figure 4. Topography (*a*) and magnetic response distribution (*b*) of the SBN60/SRO/MgO(001) heterostructure surface.

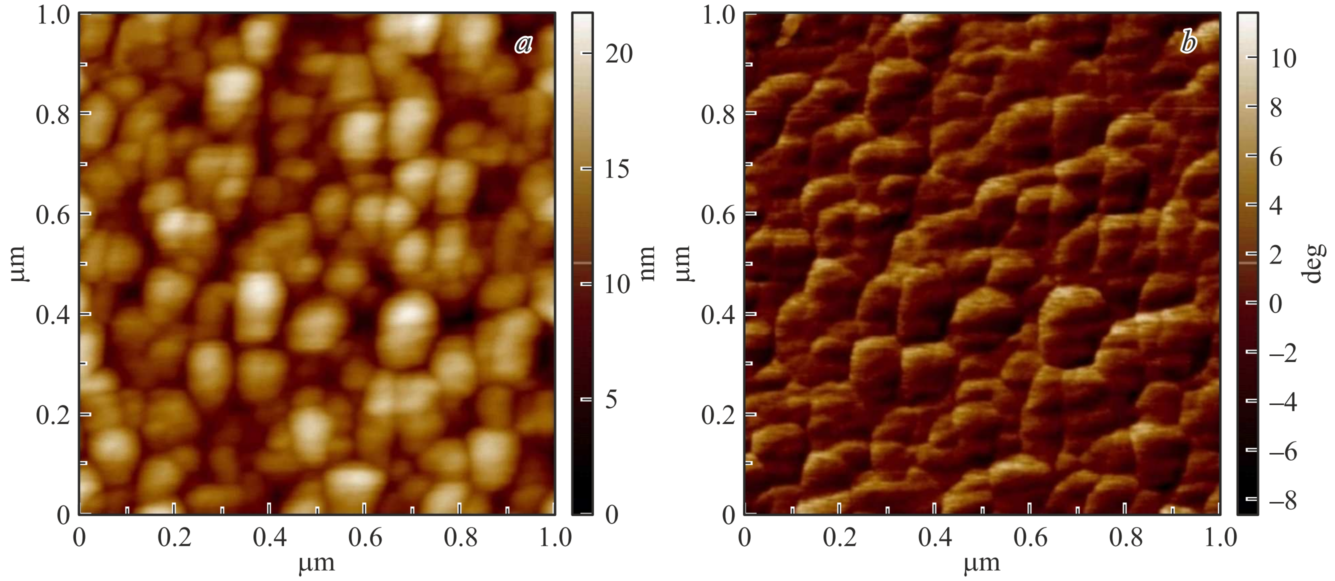

Figure 5. Topography (*a*) and magnetic response distribution (*b*) of the BFO/SBN60/SRO/MgO(001) heterostructure surfaces.

in the form of polyhedron with flat boundaries, the average size of which was 85–91 nm.

The block conglomerates formed two types of visually distinguishable surface areas, which also appeared on the height distribution histogram — if for MgO and SRO/MgO the histograms are unimodal and satisfactorily described by Gaussian distribution, then for SBN60/SRO/MgO — it is bimodal with asymmetry in the positive part of the distribution. We observed this for the first time for barium-strontium niobate films, and may be due to the following. SBN heteroepitaxial films on MgO(001) substrates, both by the used sputtering method [15,16], and by other methods [17,18], grow according to the Volmer-Weber growth mechanism with the formation of various types of orientation domains. In this case film growth occurs through the initial formation of three-dimensional nuclei, which subsequently grow into a continuous film on the surface of the substrate. During the direct growth of SBN60 on MgO(001), the film surface is homogeneous, a unimodal distribution is recorded in the histograms, and with thickness increasing Sq increases without signs of the orientation domains formation, since for the unit cells junction of the film and the substrate, these directions are equal, and the probability of the islands formation with the orientation ±18.4° is the same, respectively. When depositing SBN60 on SRO/MgO(001), this may be violated, since SRO film is characterized by its nanostructure, and probably in some places on SRO film surface it is more advantageous to form islands with growth orientation $+18.4^\circ$, while in others — with -18.4°. Further, at the stage of coalescence, when small islands combine, in the case of their identical epitaxial orientation, they merge into large blocks, and in case of different epitaxial orientation the merging will be difficult, and, in particular, mismatch dislocations may appear at their boundaries, and the surface of such blocks may just be less nonuniform. Most likely this is what we are seeing. The BFO film was also characterized by a block structure of the surface, the distribution of heights and depressions was more uniform, Sq was 2.97 nm, and the lateral size of the blocks was smaller than in SBN60 and amounted to $\sim 69-73$ nm. The histogram of height distribution for BFO/SBN60/SRO/MgO was also characterized by asymmetry, but the bimodality was less pronounced.

In single-crystal films of BFO multiferroic, the bulk material of which has a rhombohedral distorted cubic lattice, the change in the structure can lead to change in its ground antiferromagnetic state and magnetic properties. In particular, due to elastic strain in BFO films the basic and the additional uniaxial anisotropies of magnetoelastic and electrostrictive origin arise, which determine the features of the change in spin states in multiferroic depending on the degree of lattice distortion [19]. In the paper [20] it was experimentally shown that the spatial modulation of the antiferromagnetic structure in thick films of BFO multiferroic disappears not only in magnetic field, but also in its absence upon a sufficiently large mismatch of lattice constants under both compressive and tensile strain. In BFO films 1 μm thick, which have monoclinic symmetry with a slight unit cell strain, antiferromagnetic ordering with spatial spin-modulated structure (SMS) of the cycloid type is observed [21]. However, in the BFO films studied in this paper we see tensile unit cell strain, which allows us to expect change in the magnetic properties. This was revealed when measuring the magnetic response of the samples using magnetic force microscopy methods, presented in Figure 4, 5. During scanning the magnetic cantilever oscillates at a resonant frequency, and when the cantilever passes over the region of local magnetization, a shift of the cantilever oscillation phase occurs, which is registered by the microscope. Since the direction of cantilever magnetization is unknown, useful information is change in the sign of the phase shift, indicating change in the direction of local magnetization. In the obtained scans of the magnetic phase distribution of SBN60/SRO/MgO heterostructure taken for comparison, only a slight phase shift was observed over the entire surface; no correlation with the surface structure of SBN60 film was registered, this is due to the absence, as expected, of the magnetic response of the sample.

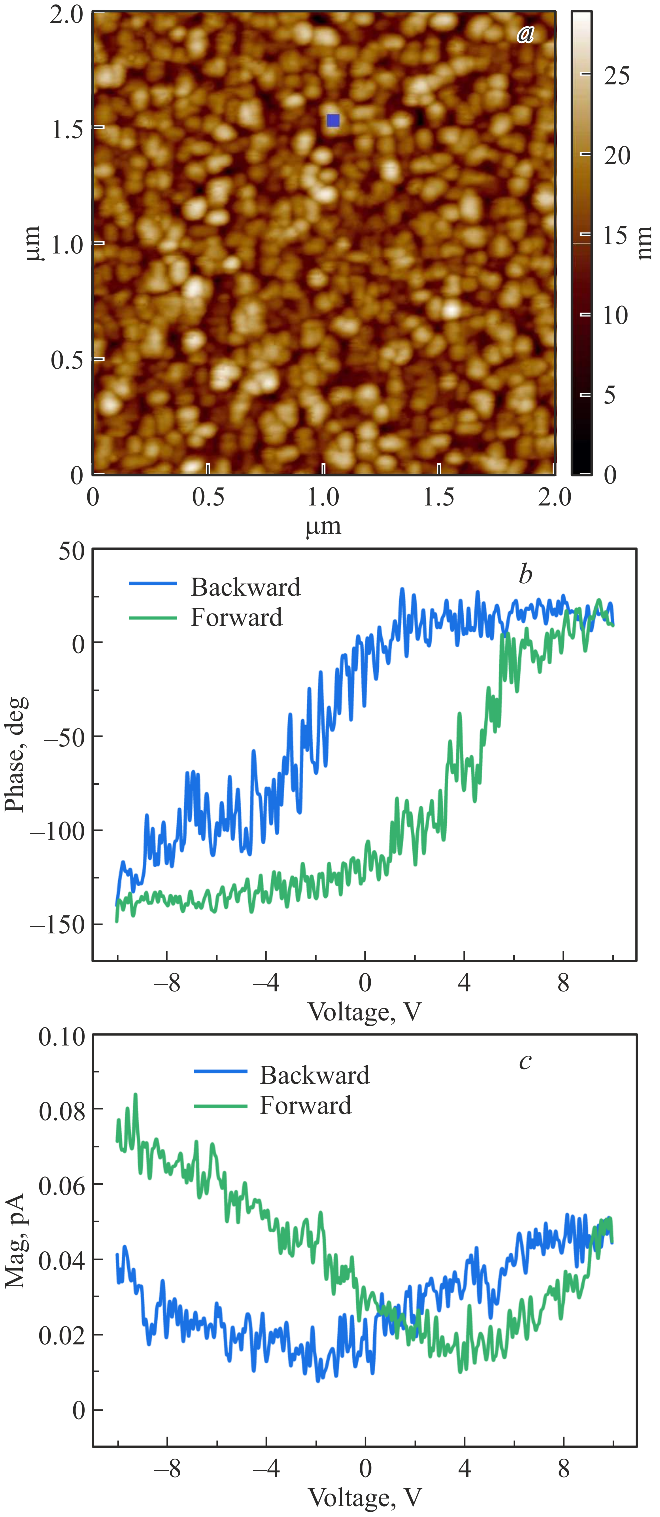

Figure 6. Surface morphology (*a*), and dependencies of phase (*b*) and amplitude (*c*) of piezoresponse on voltage obtained in PFM spectroscopy, for BFO/SBN60/SRO/MgO heterostructure. The blue square on the topography scan marks the location of measurements.

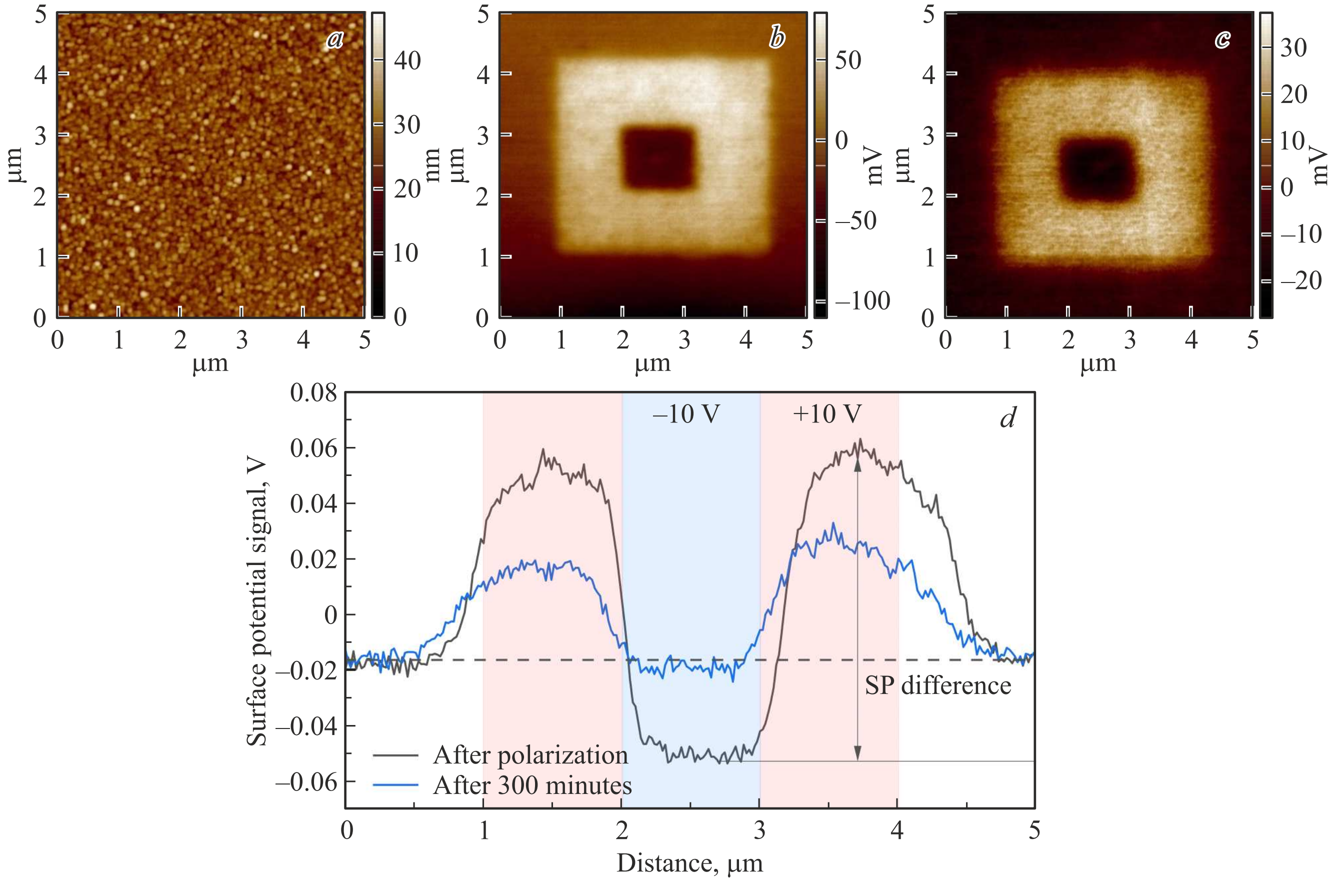

Figure 7. Topography (*a*), surface potential of the BFO/SBN60/SRO/MgO heterostructure, obtained immediately after polarization (*b*) and in 300 min (*c*) after it. *d* — profiles of the surface potential signal of BFO/SBN60/SRO/MgO heterostructure immediately after polarization (black curve) and 300 min after polarization (blue curve), drawn in the middle of the surface potential scans.

In the case of the BFO/SBN60/SRO/MgO heterostructure a radically different picture is registered — on the magnetic phase scan regions with different magnetic responses were clearly visualized, the phase difference reached 25°, however, regions of local magnetization were registered, a change sign of them occurred both at the boundaries of growth blocks and inside. This indirectly indicates a significant change in the SMS in these BFO films (may be its complete destruction), this may be associated with the features of the domain structure of BFO films as part of multilayer heterostructure. In [22] it is shown that differences in the behavior of magnetization for ferroelectric boundaries in BFOs of different types (180, 109, 71°) are associated with the features of the micromagnetic distribution, the direction of orientation of antiferromagnetic vector in ferroelectric domains, and can be explained due to the mechanism of heterogeneous magnetoelectric interaction. Taking this into account, the ferroelectric response of BFO/SBN60/SRO/MgO was studied using AFM methods. The results of studying the phase and amplitude (Mag) of the local piezoresponse hysteresis loops to the sample bias voltage are shown in Figure 6.

During the measurement typical for ferroelectric materials „loop“ of practically classic form for the phase of the local piezoresponse and „butterfly“ for the amplitude were observed with saturation already in the fields ± 10 V. Considering this in contact mode on surface of BFO/SBN60/SRO/MgO heterostructure square region with size $3 \times 3\,\mu m^2$ and $1 \times 1\,\mu m^2$ were polarized with voltage $+10$ V and -10 V (domain structure „box in box“). In the KPFM, using a two-pass technique that eliminates the topography influence on the measurement results, the areas induced during the polarization were studied using a conductive probe NSG01/Pt (Figure 7). During surface potential signal registration the probe was removed at a distance of 20 nm from the film surface.

After 300 min the induced regions were clearly observed, despite the fact that there was an asymmetry in the value of the surface potential for the regions induced with the opposite sign — the region polarized by positive voltage had a larger potential value. The potential value of the unpolarized part of the BFO film surface was ~ -0.017 V, which indicates that the domain structure in the film was initially unipolar (direction — from the substrate to the film surface). Relaxation of the region polarized by the voltage -10 V proceeds faster to the level of the unpolarized part of the film than for the region polarized by positive potential.

4. Conclusion

Thus, using the method of RF cathode sputtering the BFO/SBN60/SRO/MgO(001) heterostructures were manufactured, in which, according to both X-ray diffraction analysis and AFM data, there were no impurity phases, and all layers were grown heteroepitaxially and had high structural perfection. It was established that the growth of BFO film occurs with the formation of crystallographic axes parallel to the axes of MgO substrate and SRO layer, despite the fact that BFO layer is sputtered on top of SBN60, in which orientation domains with axes rotation by $\pm 18.4^\circ$ relative to the axes of the substrate were found. It is shown that the identified features of layer growth may be responsible for the formation of the features of their surface nanostructure. When analyzing the magnetic and ferroelectric response of BFO/SBN60/SRO/MgO(001) heterostructure using MFM and KPFM methods, it was shown that on surface of BFO film there are regions with different magnetic responses, changing both at the boundaries of growth blocks and inside the blocks, as well as the possibility of creating stable regions polarized by a constant electric field.

The results indicate that the process of polarization switching and relaxation in the heterostructure under study is quite complex, which may be associated both with the interaction between the SBN60 and BFO layers and with strain effects. For a more detailed understanding of the nature of the identified effects, it is advisable to perform studies, for example, for a series of BFO/SBN60/SRO/MgO heterostructures, in which only the thickness of the BFO layer will change. We plan to implement this in future paper.

Funding

The work was carried out as part of the President Grant MD-483.2022.1.2, with the support of the scientific project No. G30110/22-01-EP within the framework of the state assignment of the Ministry of Science and Higher Education of the Russian Federation, State Assignment of Southern Scientific Center of the Russian Academy of Sciences under the project No. 122020100294-9.

Conflict of interest

The authors declare that they have no conflict of interest.

References

[1] D. Sando, A. Barthélémy, M. Bibes. J. Phys.: Condens. Matter **26**, 473201 (2014).

[2] X. Yang, Z. Zhou, T. Nan, Y. Gao, G.M. Yang, M. Liu, N.X. Sun. J. Mater. Chem. C **4**, 234 (2016).

[3] G. Catalan, J.F. Scott. Adv. Mater. **21**, *24*, 2463 (2009).

[4] H. Béa, B. Dupé, S. Fusil, R. Mattana, E. Jacquet, B. Warot-Fonrose, F. Wilhelm, A. Rogalev, S. Petit, V. Cros, A. Anane, F. Petroff, K. Bouzehouane, G. Geneste, B. Dkhil, S. Lisenkov, I. Ponomareva, L. Bellaiche, M. Bibes, A. Barthélémy. Phys. Rev. Lett. **102**, *21*, 217603 (2009).

[5] R.J. Zeches, M.D. Rossell, J.X. Zhang, A.J. Hatt, Q. He, C.-H. Yang, A. Kumar, C.H. Wang, A. Melville, C. Adamo, G. Sheng, Y.-H. Chu, J.F. Ihlefeld, R. Erni, C. Ederer, V. Gopalan, L.Q. Chen, D.G. Schlom, N.A. Spaldin, L.W. Martin, R. Ramesh. Science **326**, 977 (2009).

[6] J.C. Yang, Q. He, S.J. Suresha, C.Y. Kuo, C.Y. Peng, R.C. Haislmaier, M.A. Motyka, G. Sheng, C. Adamo, H.J. Lin, Z. Hu, L. Chang, L.H. Tjeng, E. Arenholz, N.J. Podraza, M. Bernhagen, R. Uecker, D.G. Schlom, V. Gopalan, L.Q. Chen, C.T. Chen, R. Ramesh, Y.H. Chu. Phys. Rev. Lett. **109**, *24*, 247606 (2012).

[7] J.X. Zhang, Q. He, M. Trassin, W. Luo, D. Yi, M.D. Rossell, P. Yu, L. You, C.H. Wang, C.Y. Kuo, J.T. Heron, Z. Hu, R.J. Zeches, H.J. Lin, A. Tanaka, C.T. Chen, L.H. Tjeng, Y.-H. Chu, R. Ramesh. Phys. Rev. Lett. **107**, *14*, 147602 (2011).

[8] D. Sando, Y. Yang, E. Bousquet, C. Carretero, V. Garcia, S. Fusil, D. Dolfi, A. Barthelemy, Ph. Ghosez, L. Bellaiche, M. Bibes. Nature Commun. **7**, 10718 (2016).

[9] S. Nakashima, T. Uchida, K. Doi, K. Saitoh, H. Fujisawa, O. Sakata, Y. Katsuya, N. Tanaka, M. Shimizu. Jpn. J. Appl. Phys. **55**, 101501 (2016).

[10] J.X. Zhang, B. Xiang, Q. He, J. Seidel, R.J. Zeches, P. Yu, S.Y. Yang, C.H. Wang, Y-H. Chu, L.W. Martin, A.M. Minor, R. Ramesh. Nature Nanotech. **6**, 98 (2011).

[11] M.G. Blamire, J.W.A. Robinson. J. Phys.: Condens. Matter **26**, 453201 (2014).

[12] K.P. Jayadevan, T.Y. Tseng. J. Mater.Sci.: Mater. Electron. **13**, 439 (2002).

[13] Yu.S. Kuzminov. Ferroelectric crystals to control laser radiation. Nauka, M. (1982). 400 s. (in Russian).

[14] M. Cuniot-Ponsard Strontium Barium Niobate Thin Films for Dielectric and Electro-Optic Applications. Ferroelectrics — Material Aspects. In Tech; (2011). P. 497.

[15] A.V. Pavlenko, D.V. Stryukov, L.I. Ivleva, A.P. Kovtun, K.M. Zhidel', P.A. Lykov. FTT **63**, *2*, 250 (2021). (in Russian)

[16] A.V. Pavlenko, D.A. Kiselev, Ya.Yu. Matyash, FTT **63**, *6*, 776 (2021). (in Russian)

[17] V.H. Pedersen, A.B. Blichfeld, K. Bakken, D. Chernyshov, T. Grande, M.-A. Einarsrud. Cryst. Growth Des. **22**, 5912 (2022).

[18] A. Infortuna, P. Muralt, M. Cantoni, N. Setter. J. Appl. Phys. **100**, 104110 (2006).

[19] N.E. Kulagin, A.F. Popkov, S.V. Solovyov, A.K. Zvezdin. FTT **61**, *2*, 248 (2019). (in Russian).

[20] D. Sando, A. Agbelele, D. Rahmedov, J. Liu, P. Rovillain, C. Toulouse, I. C. Infante, A. P. Pyatakov, S. Fusil, E. Jacquet, C. Carrétéro, C. Deranlot, S. Lisenkov, D. Wang, J.-M. Le Breton, M. Cazayous, A. Sacuto, J. Juraszek, A.K. Zvezdin, L. Bellaiche, B. Dkhil, A. Barthélémy, M. Bibes. Nature Mater. **12**, 641 (2013).

[21] A.V. Pavlenko, D.V. Stryukov, S.P. Kubrin. FTT **64**, *2*, 218 (2022). (in Russian).

[22] Z. V. Gareeva, A.K. Zvezdin. FTT **54**, *5*, 1004 (2012). (in Russian).

Translated by I.Mazurov